UCRL-97433
PREPRINT

BOREHOLE GRAVITY MEASUREMENTS IN THE SALTON SEA SCIENTIFIC DRILLING PROGRAM WELL STATE 2-14

P. W. Kasameyer
J. R Hearst

This paper was prepared for submittal to
Journal of Geophysical Research

September 1987

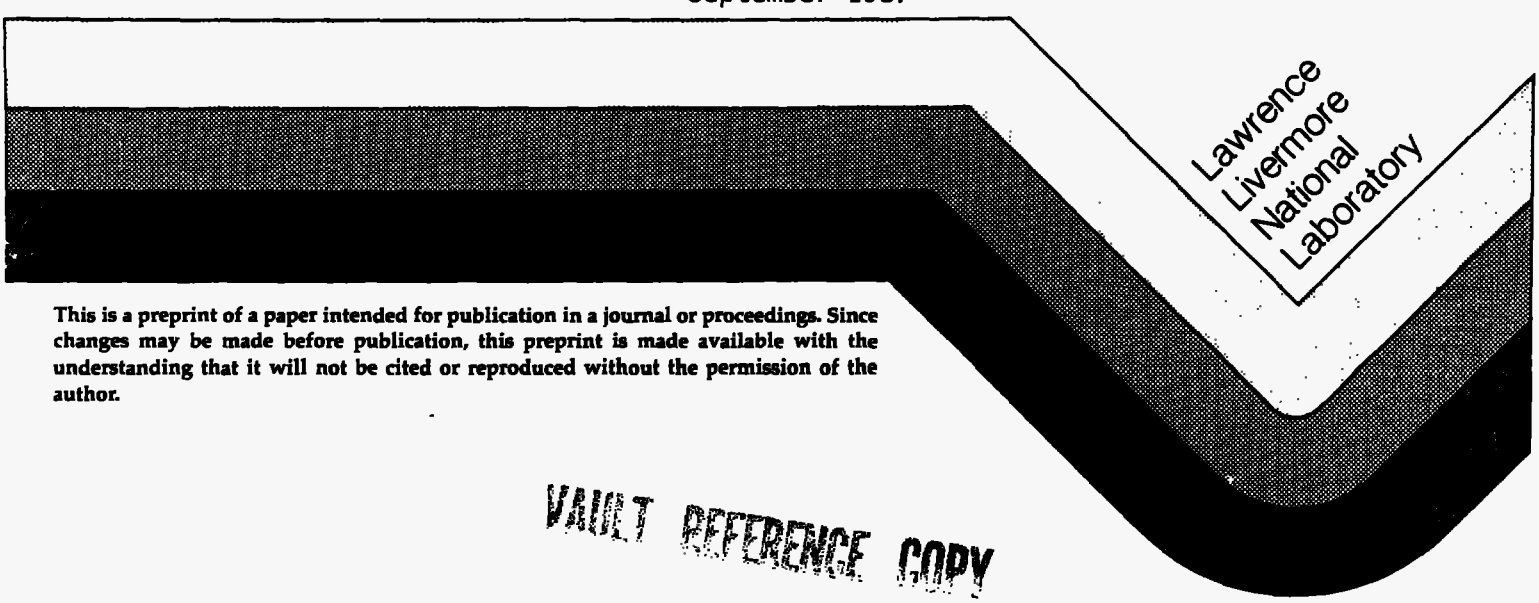

BOREHOLE GRAVITY MEASUREMENTS IN THE SALTON SEA SCIENTIFIC DRILLING PROGRAM WELL STATE 2-14 *

Paul W. Kasameyer

Joseph R Hearst

Lawrence Livermore National Laboratory

Submitted to the
Journal of Geophysical Research
September 22, 1987

*This work was performed under the auspices of the U.S. Department of Energy by Lawrence Livermore National Laboratory under contract No. W-7405-Eng-48.

ABSTRACT

Borehole gravity measurements over a depth range from 1737 to 1027 m, and the vertical gradient of gravity were measured at the Salton Sea Scientific Drilling Program well State 2-14. The borehole gravimetric densities matched the well logs, but the surface gradient was found to be 0.0040 mgal/m higher than expected. When the borehole observations are corrected for the observed free air gradient above ground, they produce densities which are nearly uniformly higher than log densities by about 0.07 gm/cm^3. These measurements require densities in the depth range .5 to 3 km, for a radius of a few kilometers around State 2-14 to be as dense as those found in State 2-14. Combining the borehole gravity and calculated vertical gravity gradients on the surface, we find that this densified zone covers much of a broad thermal anomaly to the northeast of the Salton Sea Geothermal Field.

INTRODUCTION

The Salton Sea Scientific Drilling Program (SSSDP) has drilled a borehole into the hydrothermal system at the Salton Sea Geothermal Field, an interesting scientific target. Elders, *et al.* (1972) have shown how the Salton Trough was formed over the last four million years by oblique relative motion between the Pacific and North American plates, and have identified a number of pull-apart zones where the spreading appears to be concentrated at present. The northernmost pull-apart zone lies under the Salton Sea Geothermal Field (SSGF), the largest, hottest geothermal system in the Salton Trough. Here, young sediments are being modified by heat and material from the mantle to augment the

continental crust. The SSSDP provides the opportunity to understand the system's thermal and chemical evolution, and ultimately to learn about the nature of this process of crustal development

Density is an important property measured in the SSSDP drillhole. Muramoto and Elders (1984) have described the importance of density for understanding geothermal systems in the Salton Trough. The trough is filled with young deltaic sediments, whose density would normally be expected to increase with depth along well-known compaction curves. In the geothermal systems, the sediments have undergone substantial alteration and metamorphism, and are much denser than is predicted from compaction curves. Muramoto and Elders used the increase in bulk density with depth for both sand and shales, and resistivity logs, to identify zones of increasing thermal alteration with depth in the wells from the SSGF, and to infer the maximum temperature seen by the sediments. The SSSDP well, State 2-14, provides the opportunity to extend these studies with an extensive set of cores, cuttings and well logs.

Because density in the Salton Trough is diagnostic of the degree of alteration, it is well correlated with temperature. As a result, routine gravity surveys (i. e. Biehler, *et al.* 1964) have provided the means to identify potential geothermal fields. This approach is so successful that Combs (1971) reports that there is a one-to-one correspondence between gravity anomalies and thermal anomalies in the Imperial Valley. The SSGF is covered by a +20 mgal gravity anomaly which is inferred to be caused by a

combination of high density from altered sediments and possible deeper intrusions (Biehler, *et al.*, 1964). Because of the ambiguity inherent in gravity interpretation, surface measurements cannot distinguish between a laterally extensive, near-surface density anomaly and a deeper, more concentrated body. Interpretation of the logging and detailed sampling of State 2-14 will provide additional constraints on the density distribution with depth.

The State 2-14 lies near the edge of a zone of high heat flow inferred to mark the active convecting portion of the hydrothermal system, and therefore, might be near the edge of the zone of high density sediments. A borehole gravity survey was planned to place constraints on the distance to this edge, and therefore on the depth distribution of anomalously dense sediments. In this paper we describe the results of that survey and their implications for the thermal history at the Salton Sea Geothermal Field.

THERMAL STRUCTURE OF THE SALTON SEA GEOTHERMAL FIELD

The temperature distribution in the SSGF is discussed in papers by Newmark, *et al.* (1987) and Sass, *et al.* (1987) in this volume. Newmark *et al.*, (1987) report on shallow thermal gradient measurements surrounding the SSGF, and identify four zones with distinct heat flows representing the dominance of different mechanisms of thermal transport. (Figure 1) The largest zone covers most of the Imperial Valley, which Lachenbruch, *et al.*, (1985) recognized has an anomalously high thermal gradient of about 0.07 ^{o}C/m. Surrounding the SSGF on at least three sides is a broad zone with nearly conductive temperature profiles and a

typical gradient of 0.10 ^{o}C/m. This zone has been drilled in two areas, the Westmorland Field, to the southwest of the SSGF, and the Niland Field, east of the center of the SSGF. The axis of the geothermal field is identified by a 4 km wide, uniform zone with surface gradient of about 0.4 ^{o}C/m. Decreasing gradients at depth imply convective transport in this zone. Finally, within the axial zone are two localized, intense convective zones, with gradients as high as 0.8 ^{o}C/m, called the Mullet Island anomaly and the Kornbloom Road anomaly.

State 2-14 lies on the outer boundary of both the Mullet Island localized anomaly. and the axial heat flow zones, where the heat transport is inferred to be dominated by hydrothermal convection. Sass, *et al.* (1987) report on thermal measurements in the State 2-14, which has an unusually high near-surface gradient, perhaps associated with the Mullet Island anomaly, and below 150 m has temperatures intermediate between wells within the axial zone and wells in the broad conductive zone.

DENSITY LOGS FROM THE SSGF WELLS

Muramoto and Elders, 1984, examined the changes in resistivity logs and gamma-gamma density logs with depth in the SSGF to study the mechanisms and distribution of alteration within the geothermal field. They developed empirical relationships to enable them to infer the degree of hydrothermal alteration from examination of the logs. Figure 2 shows idealized shale density profiles based on their data from the northeastern part of the axial anomaly, (wells Magmamax #2 and #3) and the southwestern portion of the broad anomaly (Landers #1 and #2, and Dearborn

Farms #1). Also shown are idealized temperature profiles for these same zones, from Newmark, *et al.*, (1987). Muramoto and Elders concluded that within the axial portion of the field, different ranges of shale density are associated with each zone of alteration, and therefore each temperature interval. In the illite zone, where temperatures rise from below 190 C to about 240 C, the shale density increases from 2.15 to 2.25 gm/cm^3 and the sand density increases from 2.05 to 2.2 gm/cm^3. The chlorite zone, from about 240 C to 295 C, is represented by shale densities increasing from 2.25 to 2.6 gm/cm^3 and sand densities rising from 2.2 to 2.4 gm/cm^3. Conversely, a shale density of 2.15 is diagnostic of temperatures near 190 ^oC, 2.25 is diagnostic of 240 ^oC and a rise in shale density to 2.6 is diagnostic of temperature near 295 ^oC. At each depth, densities in the southwestern broad anomaly are lower, consistent with the observed lower temperatures.

Temperature data (Sass, *et al.*, 1987) and density data from State 2-14 are included in Figure 2. The temperatures are lower than in the axial anomaly, but the density-depth curve data are similar to that seen within the axial anomaly. The gamma-gamma density data were obtained with a standard Schlumberger compensated density log (FDC) as is described in Paillet, 1987. The performance of this tool is discussed in Hearst and Nelson (1985), section 6.4. The shaded area in Figure 2 encompasses all density values for which the compensation to the density was less than 0.07 gm/cm^3, points with higher compensation being suspect. No attempt has been made to separate sand and shale lithologies for this plot; rather, it is assumed that the shale densities lie

along the higher density edge of the shaded zone, which is co-incident with the shale densities from the axial zone.

Using the density-temperature relationship described above, we have used the density log to infer paleo-temperatures, shown as dots in Figure 2,- at three depths for State 2-14. The resulting temperatures are much closer to the temperature-depth profiles seen along the axial anomaly than the observed temperatures in State 2-14. This observation is consistent with conclusions of Andes and McKibben (1987) who inferred that paleo-temperatures were 40 to 100 C higher than present temperatures based on fluid inclusions from veins in State 2-14, and Sturtevant and Williams (1987) who found that the calcium isotopic profile was similar to that observed in the higher gradient wells in the center of the SSGF.

A similar density-depth relationship is suggested in a borehole farther to the northeast in the broad anomaly. Muramoto and Elders (1984) noted that the Britz #3 density logs, which only were reported between 200 and 1000 m depth, showed anomalously higher densities than could be predicted from the observed temperature-depth curves, which are similar to those from Westmorland. Idealized shale density from Britz #3 is also shown in Figure 2.

The density data show that although State 2-14 is situated off the edge of the axial thermal anomaly, its densities are as high as any measured in the SSGF. These high densities suggest that in the past it was as hot as the axial zone. Borehole gravity provides the means to determine how far from State 2-14

the densified zone extends.

THE USE OF BOREHOLE GRAVITY IN INFER LATERAL CHANGES IN DENSITY

A gamma-gamma density log and a borehole gravimeter are often used together to infer lateral changes in density that do not intersect the borehole (Hearst and Nelson, 1985, p. 358). The interpretation approach is based on the gravity response for an infinite slab of density [RHO]. Above and below the infinite slab, the gravity is constant, and the difference in gravity measured at the top and bottom of the slab is given by

$$[\Delta]g/[\Delta]z = -4[PI][RHO] \qquad (1)$$

where [DELTA]z is the depth difference for the measurements and z increases downward. Suppose we can divide the actual density distribution within the Earth into four components

$$[RHO](x,y,z)=[RHO]_W(x,y,z)+[RHO]_L(z)+[RHO]_A(x,y,z)+[RHO]_R(x,y,z) \qquad (2)$$

where the subscripts have the following meanings:

W = of the rotating oblate spheroid Earth which produces the free-air anomaly F_W given by the formula of Heiskanen and Vening Meinesz, (1958)

L = of a set of infinite, flat-lying layers passing through the wellbore

A = of local anomalous masses which we intend to model

R = of regional masses outside the zone we intend to model.

Following the approach of Mueller, (1960), as cited by

Beyer, (1971), we assume that the regional masses are distant enough that their effect on the gradient is constant over the depth of the hole

In the following equations, all measurements locations refer to depth within the borehole, so the x and y parameters are omitted. The observed gravity difference, identified by the subscript O, at depth z in the borehole is the sum of the contributions of the four density components:

$$[DELTA]g_O(z)/[DELTA]z = F_W - 4[PI]k[RHO]L + [DELTA]g_R/[DELTA]z + [DELTA]g_A(z)/[DELTA]z \quad (3)$$

where the contribution from the term representing the layer density has been converted using equation 1. We divide the gravity gradient terms on the right-hand side of equation (3) by -4[PI]k to express them in terms of their density effect, $[RHO]^*(z)$ at depth z. The superscript "*" is used to distinguish the gravitational effect of a mass from its actual density, or the density measured by a log.

If there were no regional and local anomalies, the last two terms on the right-hand side of (3) would be zero, and the density-depth distribution could be estimated from the gravity measurements using the standard formula for gravimetric density:

$$[RHO]_O(z) = 1/4[PI]k\ (F_W - [DELTA]g_O(z)/[DELTA]z) \quad (4)$$

where F_W is the free-air gradient usually calculated from latitude and elevation using the standard free-air gradient formula (Heiskanen and Vening Meinesz, 1958) with constants given by

Robbins (1978). The density log, $[RHO]_{LOG}$, measures the the layered density plus any anomalous masses that intersect the borehole. The difference between the gravimetric density and the density measured by the log, can be derived from equations (3) and (4)

$$[RHO]_O(z)-[RHO]_{LOG} = [RHO]^*_A(z) - [RHO]_A(z)+ [RHO]^*_R \qquad (5)$$

From equation 5, we see that the anomalous mass contributes two terms to the gravity anomaly, its gravitational effect may be counterbalanced by the density of the portion of the anomalous mass along the borehole.

To identify lateral changes in density, the gamma-gamma densities are averaged over the gravity station intervals, and then the difference between gamma- gamma densities and gravimetric densities is computed. That observed difference in density is compared to the difference between calculated apparent density and the input density for a hypothetical model -- either a simple geometrical shape such as a sphere or a fault or a complex subsurface structure -- and the model is varied until the agreement between the observed and calculated values is good enough to satisfy the interpreter.

Equation (5) illustrates that, as in most gravity problems, if regional effects are not adequately removed, they contaminate the anomaly to be modelled. One way to remove the effects of regional masses is to subtract the estimated density calculated from the gradient observed above the ground surface, where the density of air can be neglected, from the gravimetric density. Using the assumption stated above that the regional vertical

gradient is constant, our new observation becomes the corrected gravimetric density,

$$d[RHO]_O(z) = [RHO]_O(z) - [RHO]_O(0) \qquad (6)$$

and the corrected gravimetric anomaly is again found by subtracting the log density

$$d[RHO]_O(z) - [RHO]_{LOG}(z) = [RHO]_A^*(z) - [RHO]_A(z) - [RHO]_A^*(0) \qquad (7)$$

Equation 7 describes the relationship between two factors:

1. on the right-hand side is the actual anomalous density within the Earth, as is reflected in its density effect at the surface and at depth and its density along the borehole

2. on the left-hand side are the observations, reflected in the density effects of the observed gradients at the surface and at depth, and the well log

To interpret the observations, we seek a model that fits equation 7. We vary our model of the anomalous mass within the earth, until the difference between its density effect and its density at depth and at the surface matches the corrected gravimetric density.

MEASUREMENTS

The gamma-gamma density measured in State 2-14 from 914 m to 2744 m is shown as the curve marked RHOB in Fig. 3. The collection and processing of this data are described in Paillet,

1987. The gravimetric density was obtained from a gravimeter survey conducted by EDCON, Inc. in March, 1986. The field procedures and analysis are described by Edcon (1986). Measurements started at a depth of 1737 m, near the bottom of the production casing, and were stopped at 1027 m because of difficulties with the equipment. A total of 46 readings were taken with the instrument clamped at 36 different depth stations, selected to encompass zones of uniform density as determined from the density log; the results are displayed in Table I. The gravity data were corrected for drift and tide by standard methods (EDCON, 1986); no terrain correction was required at this site. Drift corrections were made by reoccupying stations approximately every half hour, and requiring the gravity readings to agree. Uncertainty of drift-corrected density is estimated to vary between 0.001 and 0.007 gm/cm^3, as seen in Table I.

The gravimetric density, calculated from equation 4, is overlaid on the gamma-gamma density curve in Fig. 3. Because the two density values are so close, the gravimetric density is repeated, shifted by 1.0 gm/cm^3, to make it visible. Several details of the log density are matched by the gravimetric density, for example, step changes at 1570, 1271 and 1173 m, indicating that the depths of the two measurements were well aligned. The values of gravimetric density minus gamma-gamma density data, are shown in Fig. 4. Each point represents the center of the gravity station interval. Points marked by a cross are unreliable; the gamma-gamma data are suspect because the gap and mudcake compensation (determined from the comparison of the count rates in the two detectors of the density sonde) is greater than 0.07

gm/cm^3, the maximum value we were willing to consider acceptable. Except in the interval from 1289 to 1338 m, the gravimetric density is higher than the log density, a somewhat surprising result given the high densities seen by the log. The mean difference between the gravimetric and gamma-gamma densities is 0.02+/- 0.01 gm/cm^3. The uncertainty of individual values of the gamma-gamma density can be as high as 0.05 gm/cm^3, because of the presence of uncompensated gaps between the sonde and the borehole wall. The mean difference uncertainty was estimated by dividing this value by the square root of 28, the number of points. This difference is near the limit of the density log's calibration uncertainty for water content and for unusual temperatures, and may not be different than zero.

The uncorrected gravimetric density shows evidence only of a very weak positive anomaly over the depth range measured. From equation (5) we see that two cases are possible. In the first case, either there is no anomalous mass that influences the gradient over the depth range studied, or the anomalous mass extends so far from the borehole that its calculated gravity effect is the same as the anomalous density. Alternatively, the anomalous mass may produce a uniform gravity gradient that is cancelled by a regional anomaly of opposite sign.

The second alternative is investigated by removing the gradient above the surface from both the observations and the model, as is shown in equation (7). The gravity gradient above the surface was found to be anomalous by two independent means, directly by measurements on the drill rig, and indirectly from surface gravity measurements within 100 km of State 2-14.

M. R. Millett and D. J. Felske of LLNL measured the free-air gradient at this site by occupying gravity stations on the drill rig at heights 8.1 m and 24.3 m above ground surface. Their measurements are reported in Table II. The measured free air gradient was 0.3128 mgal/m, 0.0040 mgal/m more than F_W which is 0.3088 mgal/m.

Measured gradients can be disturbed by very local features, such as the mass of the drill rig, mud pits, and subtle local topography (Beyer, 1971). To determine if our measured gradient is disrupted by local features, we used a method described by Beyer to calculated the anomalous free-air gradient from surface gravity measurements surrounding State 2-14. We selected all the Bouguer corrected within a 100 km radius of State 2-14, using a data set compiled by NOAA, (unpublished data). These data were averaged over 20 degree azimuth zones within 15 distance rings with outer radii covering a geometric series from 1 km to 100 km. The average of the filled zones in the each ring was used to estimate the average gravity value as a function of distance, and the gradient at the surface due to anomalous and regional masses was calculated from using Beyer's equation 14.

The locations of the gravity data and contours based on the data are shown in Figure 5, and the calculated gradients are shown in Figure 6. The calculated vertical gradient at State 2-14 was 0.0043 mgal/m. within 10% of the measured value, raising our confidence in the applicability of the measured value.

Using this measured free-air gradient, the corrected

gravimetric density is larger than the uncorrected value by almost 0.05 gm/cm^3, giving an average anomaly of 0.07 gm/cm^3, a significant value. Figure 3 shows this anomaly. The anomaly curve is dashed at depths where the gamma-gamma density uncertainty is large. Equation (7) shows that this nearly uniform anomaly could be produced either by a model with a positive density effect (at depth) that exceeds its assumed density or with a negative density effect at the surface.

MODELLING

For modelling, we take the measured value of the corrected gravimetric anomaly (in Equation. 7) to be 0.07 gm/cm^3, and constant with depth. Since the surface gravity anomaly contours (Figure 5) are somewhat circular, we chose to restrict our models to cylinders with a vertical axis at the center of the surface gravity anomaly, 3962 m from the borehole. Gravity values were calculated along a vertical line parallel to the axis, using the formulation of Singh (1977). The terms on the right-hand side of Equation 7 were calculated for different sets of the parameters depth, thickness, density contrast and radius.

The anomaly of 0.07 gm/cm^3, obtained by using the corrected gravimetric density, is a surprising result in view of the high densities and high shale content observed in State 2-14, and the expectation that cooler regions surrounding it would have lower density. This anomaly could be explained by two trivial models: The first has infinite horizontal layers with density 0.07 gm/cm^3 larger than the gamma-gamma density. The observed log values would then be produced by an anomalous mass of -0.07 gm/cm^3 right

at the borehole. The second requires the presence of a large amount of high-density material near the borehole, filling much of the region between 1027 and 1737 m. Additional constraints would be needed to determine the diameter of the zone of dense material and its density. There is no geologic basis to argue for the reality of these models. They would be reasonable if State 2-14 had a greater proportion of lower density sand than surrounding wells, but it is quite shaley. We seek models that fit some independent geological constraints.

Models with excess mass outside of State 2-14

In Figure 2, we see that the density from State 2-14 is very similar to values observed in the axial portion of the geothermal field. The highest log values detected in the field, from Magmamax #2, (incorrectly labeled in Muramoto and Elders, 1984, Figure 43, as Magmamax #3), are no more than 0.1 gm/cm^3 greater than the shale densities at State 2-14. We modelled this excess density as a cylinder extending over a depth range of 500 to 3000 m with density contrast of 0.1. Figure 7 shows the calculated corrected gravimetric anomaly that would be seen in State 2-14, as a function of the radius assumed for the excess mass. Excess density in the center of the field can cause a positive anomaly, but not as large as the one observed.

Other possible sources of excess mass in the depth range studied are possible, but their geometries and density contrasts are not constrained by other data. These possibilities include dense intrusions, intense alteration at the Mullet Island thermal anomaly, and lithologic changes such as a drastic increase in

shale content. One or more of these features could be invoked to explain the observed corrected gravimetric anomaly.

Models where State 2-14 lies within the anomalous mass

Since State 2-14 has a high proportion of high density shale, we have examined models with a high density anomalous mass that encompasses the well. Of course, the outer boundary of this mass would cause a negative gravimetric anomaly, the opposite of what was detected. But, that subsurface mass anomaly also affects the measured free-air gradient, in some cases producing a negative density effect at the surface. If the negative density effect at the surface is larger than the negative effect at depth, a positive corrected gravimetric anomaly will be produced. It would be sensible to model this situation in detail if we had collected borehole gravity data near the surface to provide constraints on the model. Without such constraints we can make only simple models that indicate what is required to fit the data.

Models with a shallow anomalous cylinder can produce the corrected gravimetric anomaly that was detected. A cylinder whose outer edge is close to but beyond the borehole produces an anomalous gradient at the surface. Figure 7 shows that the corrected gravitational anomaly of 0.07 gm/cm^3 can be produced for a particular set of cylinder parameters. For this plot, labelled "shallow", we arbitrarily placed the cylinder top at 50m and bottom at 500m. If the bottom were much deeper, this model would cause variations in the anomaly over the depth range where we detected it to be constant. Figure 7 shows that, if it ends within a few hundred meters of State 2-14, a shallow body could

produce our observed corrected gravitational anomaly. This was the basis of an earlier published claim that we may have detected a shallow edge of the densified zone (Kasameyer, and Hearst, 1986). However, all shallow models that produce a high surface gradient at State 2-14 produce very large changes in vertical gradient as a function of distance, inconsistent with the smoothness of the calculated vertical gradients (Figure 6). This variability is illustrated in figure 8 for a particular shallow model with the boundary 338m from State 2-14. Based on our smooth calculated vertical gradients, we now reject near surface features as a means to produce the observed positive corrected gravimetric anomaly, and conclude that State 2-14 is far enough within the densely altered zone that its edge cannot be detected.

How close could the edge be and still be undetected? We calculated corrected gravitational anomalies for two types of cylinders, and plotted them in Figure 7. The depths and density contrasts were chosen based on the log density data in Figure 2, reflecting two different possible views of the density anomaly. To construct the first model, labeled "axial-normal", we noted that the geothermal field has densities about 0.45 gm/cm^3 above normal compaction curves. This contrast was applied over the depth range of 500 to 5000m, starting shallow enough to produce a uniform disturbance over the depths studied in State 2-14, and extending deep into the sedimentary section. In the second view, the axial anomaly is assumed to be nested within densities seen in the southern part of the broad anomaly, and is modeled by a cylinder with contrast 0.25, and depth range 500m to 3000m. Of course, these models produce anomalies whose sign is opposite the

detected one. If we assume that we could have detected a negative anomaly of 0.03 gm/cm^3, then the densities seen in the broad anomaly are no closer than one 1.4 km to State 2-14, and a boundary where densities return to "normal" is no closer than about 6 km.

The borehole gravity requires that material as dense or denser than that found in State 2-14 be found at least in depths from 1-2 kilometers out to a distance of at least a few kilometers. There is a strong suggestion from the vertical gradient map, Figure 6, that this distance is on the order of 10 to 15 km, where there is a zone of very rapid decrease in vertical gradient. To illustrate this, Figure 8 shows the vertical gradients calculated along an E-W line through State 2-14, and the vertical gradients over a cylinder representing the excess of the axial anomaly over the broad anomaly. Both curves have been converted to density effect. It is clear that cylindrical models can produce many features of the vertical gradient curve. Both have a broad central area with a constant negative density effect that increases and then falls to or through zero at the edge of the cylinder. The model falls off more rapidly, suggesting that the actual boundary is less abrupt or deeper. The vertical gradient map suggests that the boundary of this zone is in the vicinity of the mapped extension of the San Andreas Fault, near the town of Niland. If that is the case, it includes Britz #3, whose densities were similar to State 2-14.

CONCLUSIONS AND DISCUSSION:

The main contribution from the borehole gravity is that the

dense rocks penetrated between 1 and 2 km depth in State 2-14 must extend several kilometers from the well. There is no evidence from the borehole gravity data collected to date that the SSSDP well is near the edge of the high density zone it penetrates, suggesting that a large shallow zone has been as hot in the past as the zone on the axis of the SSGF is today. This conclusion is reinforced by the vertical gravity gradient map, which shows a broad zone of uniform gradient to the east of the SSSDP, and a zone of rapid decrease in gradient lying roughly along the a line extending southeast from the end of the San Andreas Fault Zone, just east of Britz #3.

This area encompasses the northeastern portion of the broad thermal anomaly. Our results suggest that the thermal history of this zone is quite different than the history of the Westmorland area, even though the present day temperatures are similar (Newmark, *et al.*, 1987). From the location of this zone between the plate boundary, as defined by the San Andreas fault zone, and the locus of present spreading, as is defined by the SSGF, we speculate that this shallow dense zone represents an earlier locus of spreading similar to the SSGF today. The nearly constant temperature gradient observed in Britz #3 suggests that heating at shallow depths ceased long enough ago for the area to return to steady state conduction. The present elevated temperatures could represent the residual heat from that event, or something independent of it. Assuming the cooling occurred by conduction, using a diffusivity, K, for compacted sedimentary rocks on the order of 40 m^2/yr, and a half-thickness, L, of 1500m for the thermal zone, we estimate its characteristic thermal time, L^2/K,

to be on the order of 60,000 years, and more than twice that time would be required to reach steady-state conduction. Thus, the minimum age of this paleo-thermal zone is about an order of magnitude greater than ages of 6000 to 20,000 years estimated for the axial anomaly (Kasameyer, *et al.*,1984).

FIGURE CAPTIONS

Figure 1. Locations of local(L), axial, broad, and valley-wide thermal anomalies at the Salton Sea Geothermal Field, from Newmark, *et al.*, 1988. The inset shows their idealized temperature profiles for these zones, and for sedimentary basins with Basin and Range heat flow for comparison.

Figure 2. Idealized density-depth and temperature-depth profiles for zones in the Salton Sea Geothermal Field. An approximate temperature profile for State 2-14 has been added to the idealized temperatures from figure 1. In the density plot, the solid lines represent average shale densities for the Westmorland Field (Broad(S)) and the Axial anomaly, and an estimate of the unaltered compaction curves, all from Muramoto and Elders (1984), figure 43. Density data from Britz #3 (dashed) and State 2-14 (shaded) have been added. The shaded area encompasses all density log points with small enough compensations. The three dots on the temperature plot represents estimates are estimated from the State 2-14 densities using the empirical relation developed by Muramoto and Elders, 1984.

Figure 3. Gravimetric and Log densities, with compensation, and corrected gravimetric anomaly for State 2-14 from 914 to 1829 m depth. For clarity, the gravimetric density has been plotted twice, once with 1.0 gm/cm^3 removed. The ranges indicated for the density logs indicate the span of the entire track they are plotted on.

Figure 4. Uncorrected gravimetric densities for State 2-14. The negative of the uncorrected gravimetric density is plotted as a

function of depth, with zones where the log is suspect indicated by "plus" signs.

Figure 5. Gravity station locations near State 2-14, and the contours derived from Bouguer corrected observations at these locations. The data were obtained from NOAA, and are very consistent with the gravity map of Biehler, *et al.*, 1964. The contour interval is 5 mgal.

Figure 6. Vertical gravity gradients estimated from surface gravity measurements within 100 km of State 2-14. The method of calculation is discussed in the text. The contour interval is 0.001 mgal/m.

Figure 7. Calculated corrected gravimetric anomaly at State 2-14 as a function of cylinder radius, for a number of cylindrical models. All cylinders are centered 3962 m from State 2-14. The Axial-State model has a density contrast of 0.10 extending from 500 to 3000 m depth. The shallow model has a contrast of 0.45 over 50 to 500 m depth. The Axial-Broad model has a contrast of 0.25 over depths from 500 to 3000 m. The Axial-normal model has a contrast of 0.45 over 500 to 5000 m depth. Only the shallow model produces the observed positive anomaly of 0.07 gm/cm^3.

Figure 8. Calculated vertical gradients at the surface, as a function of distance from the center of the cylinder, for two models that produce the correct anomaly at State 2-14. All gradients have been converted to density effect. The curve labeled "calculated from observed" identifies the calculated vertical gradient anomaly data (figure 6) along an east-west line

intersecting State 2-14. Higher distance values are to the east. The "shallow" model has a contrast of 0.45, a radius of 4300 m and covers a depth range from 50 to 500 m. The Axial-Broad model has a radius of 13 km and a contrast of 0.25 from 500 to 4000. This simple model fits the general shape of the vertical gradient data. A larger contrast and a greater thickness could match the amplitude as well.

Table I Borehole gravity Data from State 2-14

Drift-corrected, processed, borehole gravity meter data (not corrected for slant depth)

[ft, feet; mgal, milligals; g/cm^3, grams per cubic centimeter]

Depth interval (ft)	Slant delta Z	Deviation (degrees)	Delta G (mgal)	Density (g/cm^3)	80 percent confidence
5,700-5,660	40.00	0.0	1.001	2.627	0.007
5,660-5,610	50.00	.0	1.327	2.646	.007
5,610-5,520	90.00	.0	2.577	2.564	.005
5,520-5,450	70.00	.0	1.946	2.596	---
5,450-5,380	70.00	.0	1.944	2.598	---
5,380-5,290	90.00	.0	2.415	2.634	---
5,290-5,200	90.00	.0	2.454	2.617	.002
5,200-5,150	50.00	.0	1.349	2.628	.002
5,150-5,040	110.00	.0	3.184	2.551	.001
5,040-4,970	70.00	.0	2.032	2.548	---
4,970-4,880	90.00	.0	2.639	2.536	---
4,880-4,800	80.00	.0	2.317	2.550	---
4,800-4,730	70.00	.0	2.071	2.526	---
4,730-4,670	60.00	.0	1.737	2.551	---
4,670-4,580	90.00	.0	2.598	2.554	.000
4,580-4,520	60.00	.0	1.761	2.535	.000
4,520-4,460	60.00	.0	1.756	2.539	---
4,460-4,390	70.00	.0	2.000	2.565	---
4,390-4,330	60.00	.0	1.729	2.556	---
4,330-4,290	40.00	.0	1.194	2.515	.007
4,290-4,260	30.00	.0	.871	2.548	.005
4,260-4,220	40.00	.0	1.214	2.496	.003
4,220-4,165	55.00	.0	1.735	2.448	---
				[illegible]	---
4,090-4,030	60.00	.0	1.676	2.590	---
4,030-3,980	50.00	.0	1.458	2.543	---
3,980-3,885	95.00	.0	2.758	2.547	---
3,885-3,845	40.00	.0	1.194	2.515	---
3,845-3,780	65.00	.0	2.032	2.460	---
3,780-3,720	60.00	.0	1.796	2.512	---
3,720-3,660	60.00	.0	1.913	2.432	---
3,660-3,610	50.00	.0	1.554	2.467	0.002
3,610-3,550	60.00	.0	1.942	2.417	.001
3,550-3,470	80.00	.0	2.485	2.468	---
3,470-3,370	100.00	.0	3.066	2.476	---

Table 11. Gravity measurements above State 2-14

Tide corrected gravimeter data determined on April 8, 1986, by using a U.S. Geological Survey G177 meter

[hr, hour, ft, feet; mgal, milligals; mgal/ft, milligals per foot]

Time (24-h time)	Depth (ft)	Counter	Tide (mgal)	Tide correction counter	Gravity (mgal)
0700	26.60	3,207.115	-0.059	3,207.059	3,357.643
0722	106.50	3,199.834	-.045	3,199.791	3,350.035
0733	26.60	3,207.105	-.037	3,207.070	3,357.655
0743	106.50	3,199.814	-.030	3,199.786	3,350.029
0754	26.60	3,207.087	-.021	3,207.067	3,357.651
0805	106.50	3,199.798	-.012	3,199.786	3,350.029
0815	26.60	3,207.073	-.004	3,207.069	3,357.654
0823	106.50	3,199.792	.002	3,199.794	3,350.037
0832	26.60	3,207.065	.009	3,207.074	3,357.659

Average value at 26.6 ft = 3,357.652 mgal

Average value at 106.5 ft = 3,350.033 mgal

Average gravity = 7.619 mgal; Average depth = 79.92 ft

Free-air Gradient = 7.619 mgal/79.92 ft

Free-air Gradient = 0.095337 mgal/ft

REFERENCES CITED

Andes, J. P. jr., and M. A. McKibben, 1987, "Thermal and Chemical History of Mineralized Fractures in Cores from the Salton Sea Scientific Drilling Project", abst., Eos, 68, p. 439

Beyer, L. A., The Vertical Gradient of Gravity in Vertical and Near-vertical Boreholes, Stanford University Ph. D. thesis, 1971

Biehler, S., R. L. Kovach, and C. R. Allen, Geophysical framework of the northern end of Gulf of California structural province, in *Marine Geology of the Gulf of California,* edited by T. H. van Andel and G. G. Shor, jr., Amer. Assoc. of Petrol. Geol. Memoir 3, 126-143, 1964

Combs, J., Heat flow and geothermal resource estimates for the Imperial Valley, in *Cooperative Geological-Geophysical-Geochemical Investigations of Geothermal Resources in the Imperial Valley Area of California,* University of California, Riverside, edited by R. W. Rex, 1971

EDCON, INC., State well 2-14 Niland, California, Lawrence Livermore National Laboratory Report, UCRL-15945, 1986

Elders, W. A., R. Rex, T. Meidav, P. T. Robinson, and S. Biehler, "Crustal Spreading in Southern California",Science, Vol. 178, pp. 15-24, 1972

Hearst, J. R, and P. H. Nelson, *Well Logging for Physical Properties*, McGraw-Hill, New York, 1985

Heiskanen, W. A., and F. A. Vening Meinesz, *The Earth and its*

Gravity Field, McGraw-Hill, New York, 1958

Kasameyer, P. W., L. W. Younker, and J. M. Hanson, Development and application of a hydrothermal model for the Salton Sea Geothermal Field, California, Geol. Soc. Amer. Bull., 95, 1242-1252, 1984

Mueller, I. I., The gradients of gravity and their applications in geodesy, Ohio State University, Ph. D. thesis, 1960

Muramoto, F. S. and W. A. Elders, "Correlation of Wireline Log Characteristics with Hydrothermal Alteration and Other Reservoir properties of the Salton Sea and Westmorland Geothermal Fields, Imperial Valley, California, USA", Los Alamos National Laboratory Report LA-10128-MS, Los Alamos, New Mexico, 1984

Kasameyer, P. W., and J. R Hearst, Borehole gravity measurements in the SSSDP, abst., EOS, 68, 445, 1987

Lachenbruch, A. H., J. H. Sass, and S. P. Galanis, jr., Heat flow in southernmost California and the origin of the Salton Trough, J. Geophys. Res., 90, 6709-6736, 1985

Newmark, R. L., P. W. Kasameyer, and L. W. Younker, Shallow Drilling in the Salton Sea Region, submitted to J. Geophys., Res., 1987

Paillet, F. L., editor, Preliminary Report on Geophysical Well-Logging Activity on the Salton Sea Scientific Drilling Project, Imperial Valley, California, U. S. Geol. Survey, Open File Report, 86-544, 1986

Robbins, S. L., Re-examination of the values used as constants in calculating rock density from borehole gravity data, Geophysics, 46, 208-210, 1978

Sass, J.H., S. S. Priest, L. E. Duda, C. C. Carson, J. D. Hendricks, and L. C. Robison, Thermal Regime of the State 2-14 well, Salton Sea Scientific Drilling Project, submitted to J. Geophys., Res., 1987

Singh, S. K., Gravitational attraction of a vertical right circular cylinder, Geophys. J. R. astr. Soc., 50, 243-246, 1977

Sturtevant, R. G., and A. E. Williams, 1987, "Oxygen Isotopic Profiles for the State 2-14 Geothermal Well: Evidence for a Complex Thermal History", abst., Eos, 68, p. 445

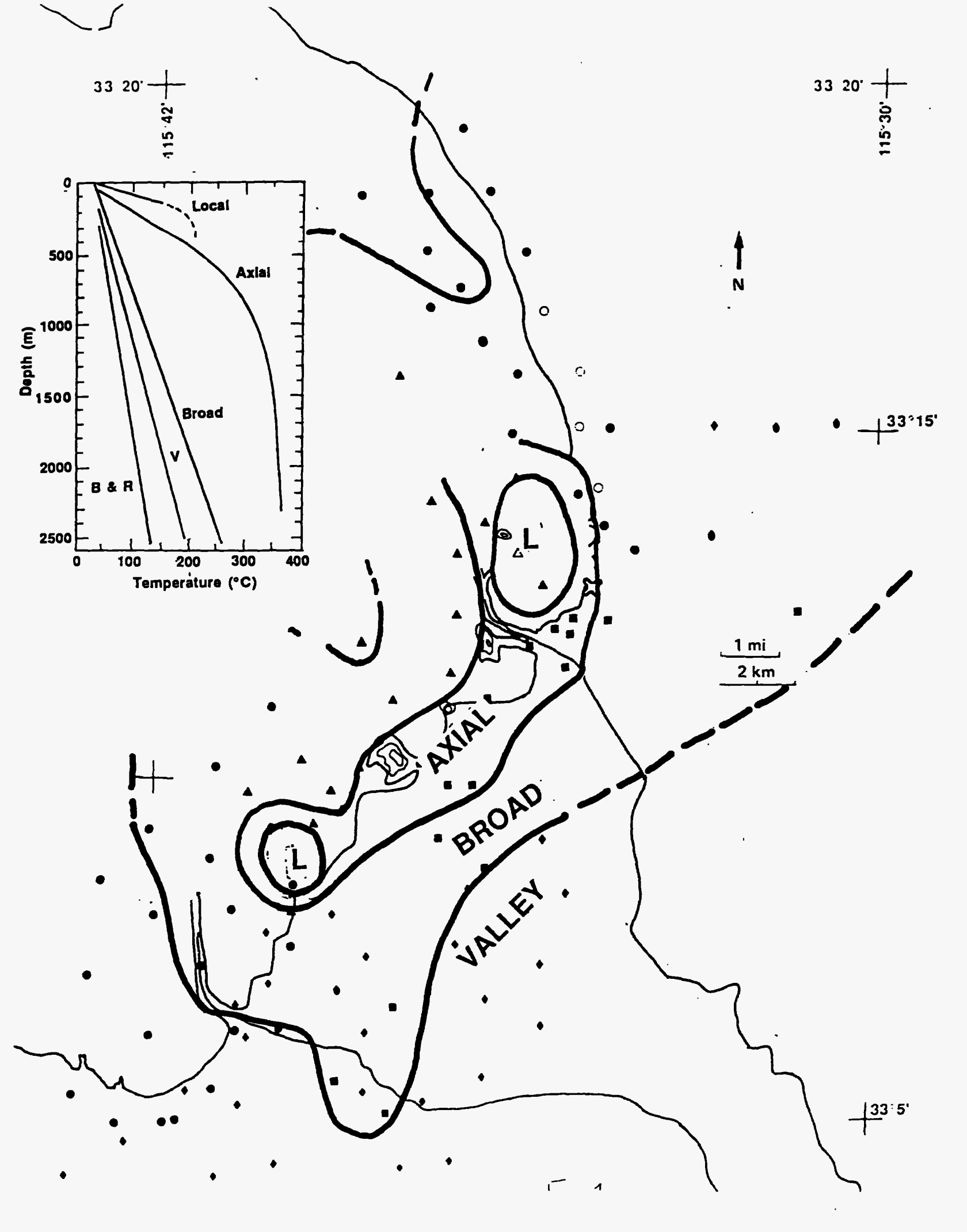
33 20'
115 42'
33 20'
115 30'
Local
Axial
Broad
V
B & R
Depth (m)
0
500
1000
1500
2000
2500
0
100
200
300
400
Temperature (°C)
N
33 15'
L
1 mi
2 km
AXIAL
BROAD
VALLEY
L
33 5'

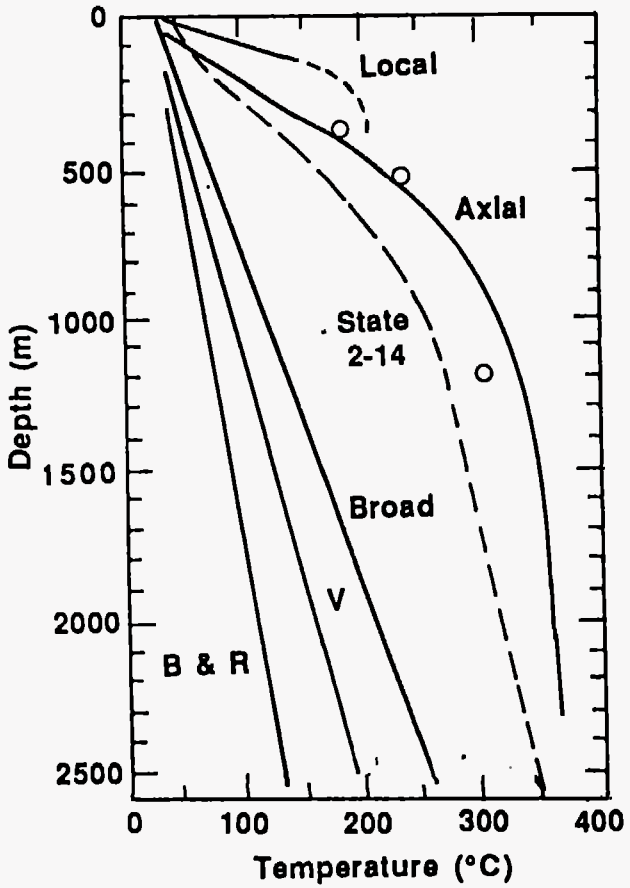
0
500
1000
1500
2000
2500
Depth (m)
0
100
200
300
400
Temperature (°C)
Local
Axial
State
2-14
Broad
V
B & R

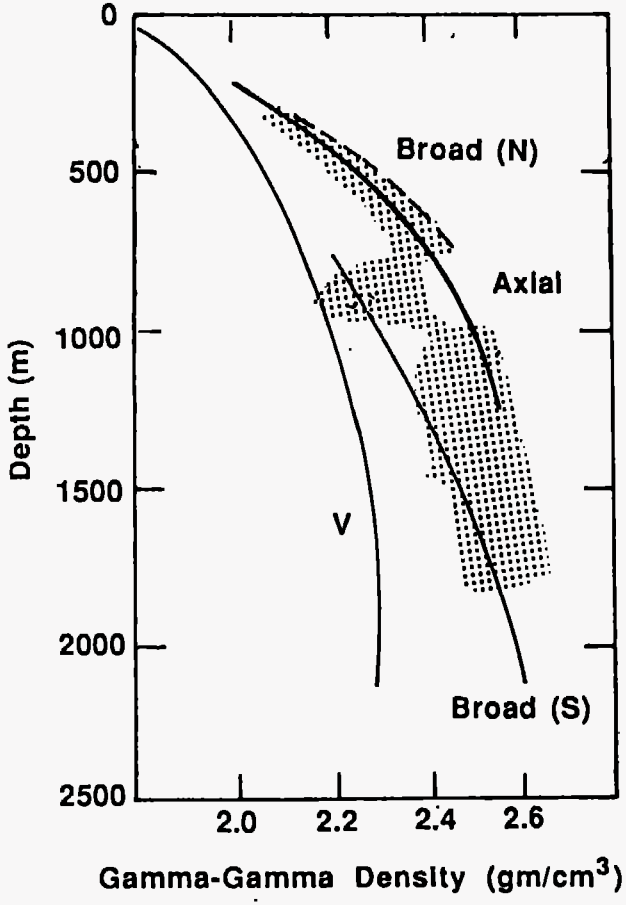
0
500
1000
1500
2000
2500
Depth (m)
2.0
2.2
2.4
2.6
Gamma-Gamma Density (gm/cm3)
Broad (N)
Axial
V
Broad (S)

STATE 2-14 SSSDP WELL

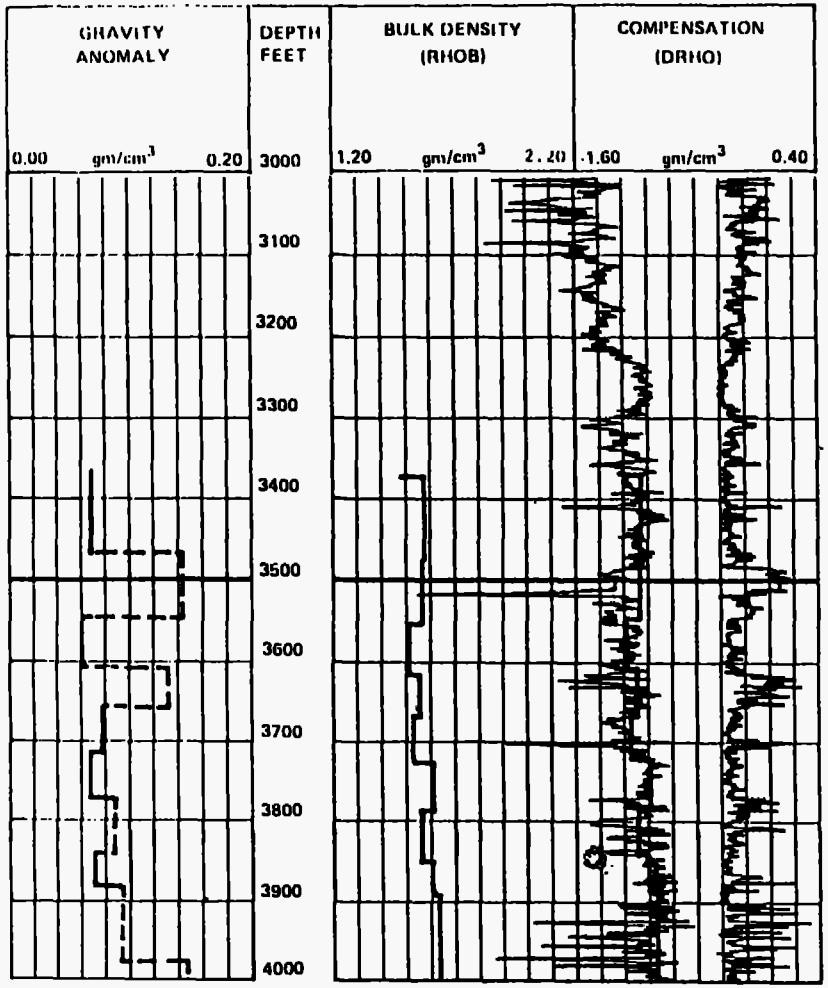

Figure 23.--Gravity-anomaly log (depth interval 3,370 to 5,700 feet) and commercial bulk-density and compensation logs (depth interval 1,000 to 6,000 feet). (Continued)

STATE 2-14 SSSDP WELL

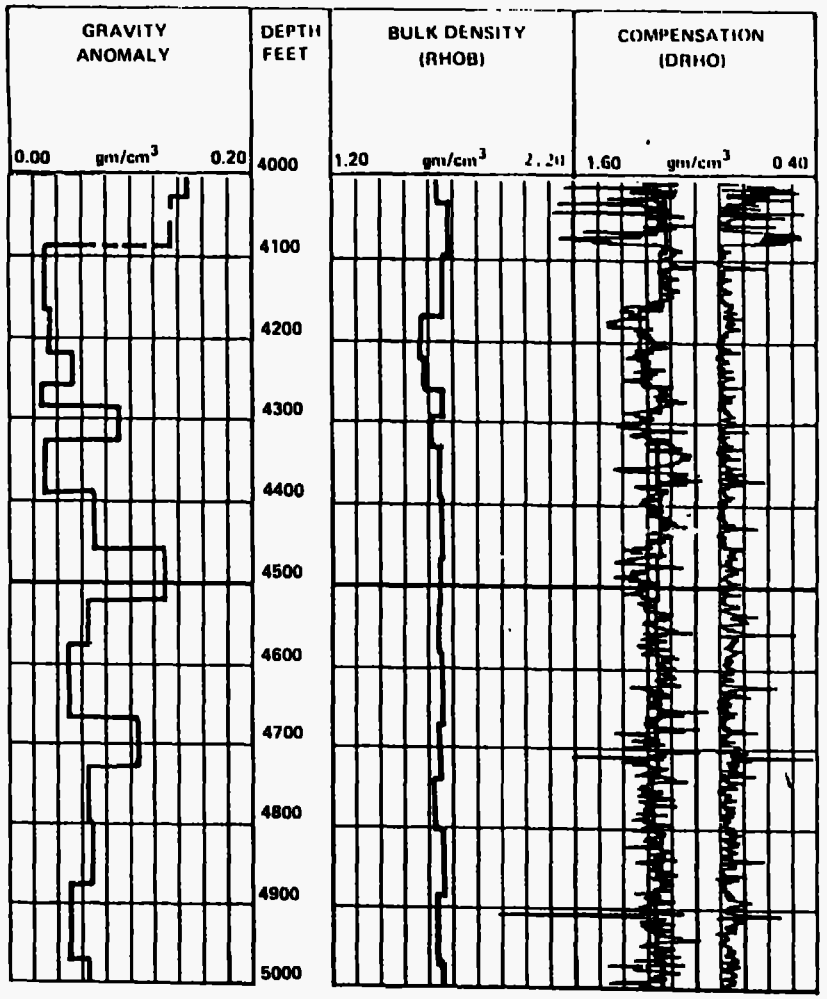

Fig 3A

Fig 3B

STATE 2-14 SSSDP WELL

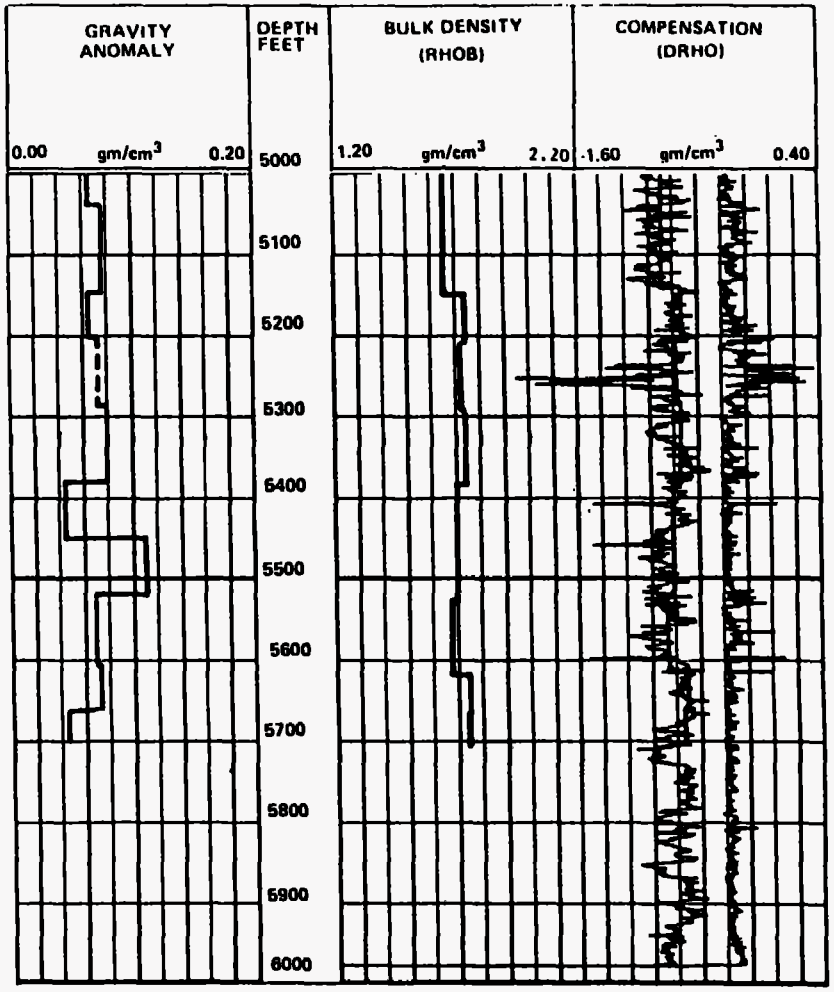

Figure 23.--Gravity-anomaly log (depth interval 3,370 to 5,700 feet) and commercial bulk-density and compensation logs (depth interval 1,000 to 6,000 feet). (Continued)

Fig 3c

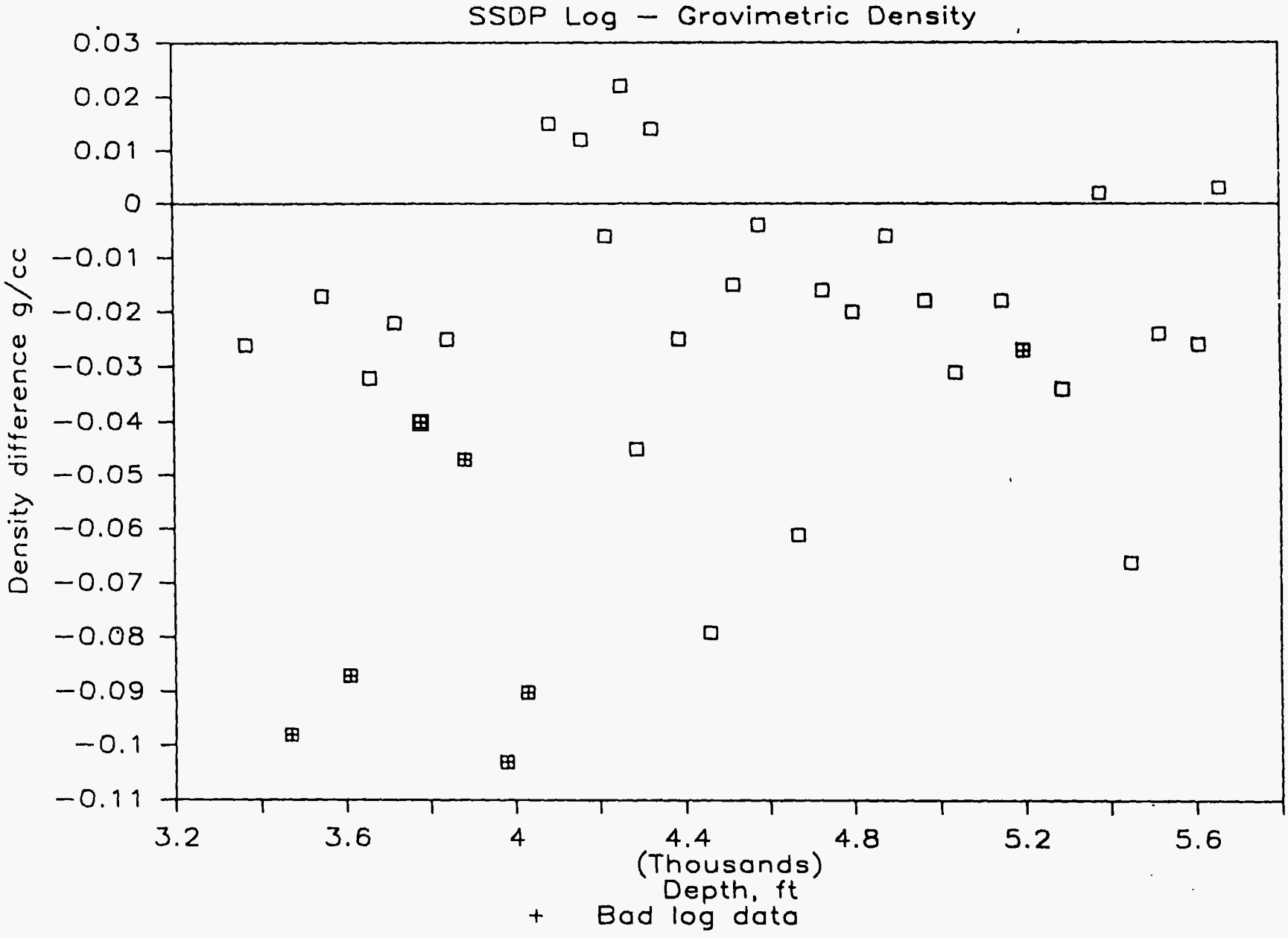
SSDP Log — Gravimetric Density
Density difference g/cc
0.03
0.02
0.01
0
−0.01
−0.02
−0.03
−0.04
−0.05
−0.06
−0.07
−0.08
−0.09
−0.1
−0.11
3.2
3.6
4
4.4
4.8
5.2
5.6
(Thousands)
Depth, ft
+ Bad log data

Fig 4

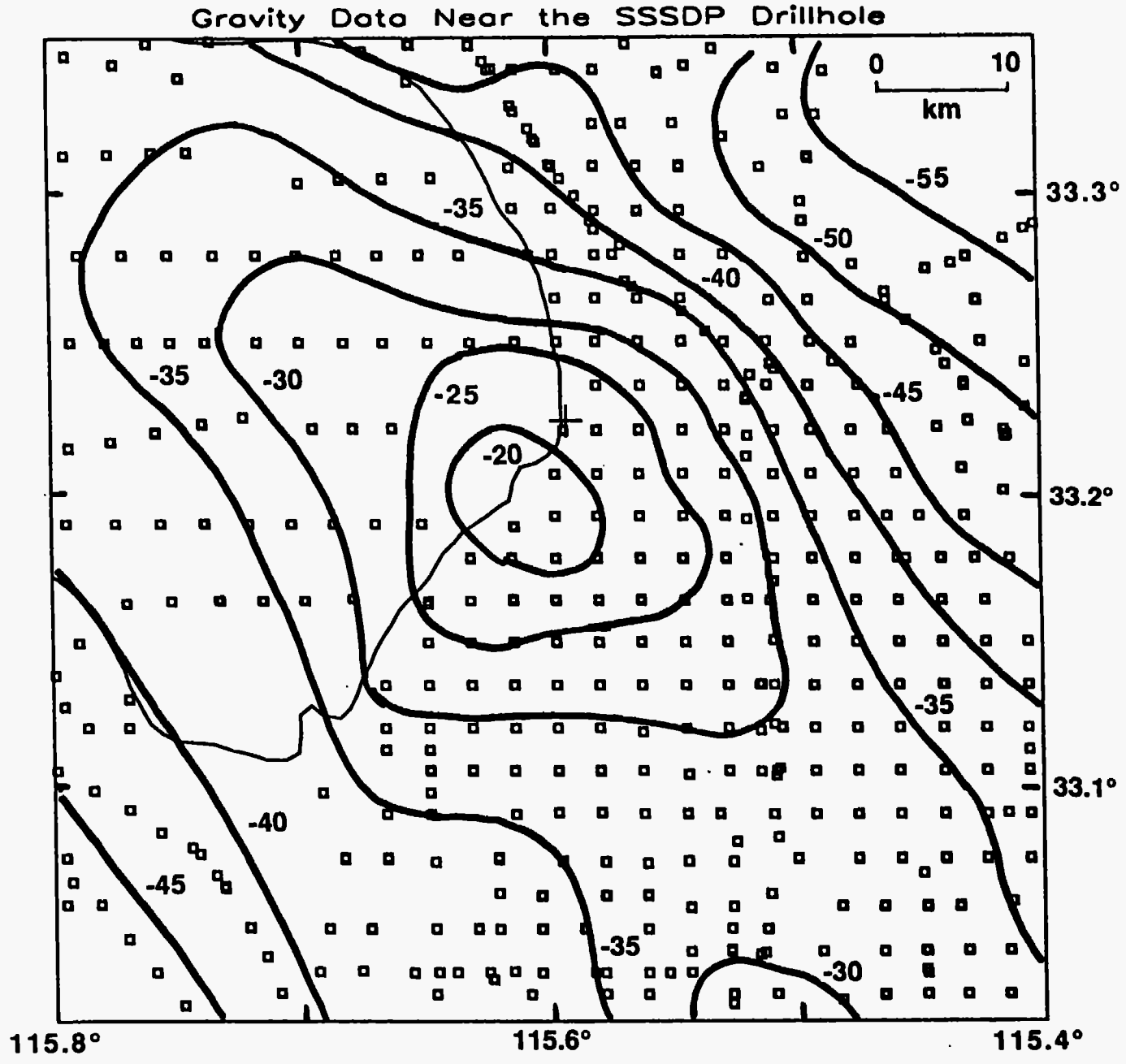
Gravity Data Near the SSSDP Drillhole
0
10
km
-55
-50
-40
-35
-45
-35
-30
-25
-20
-35
-40
-45
-35
-30
33.3°
33.2°
33.1°
115.8°
115.6°
115.4°

Fig. 5

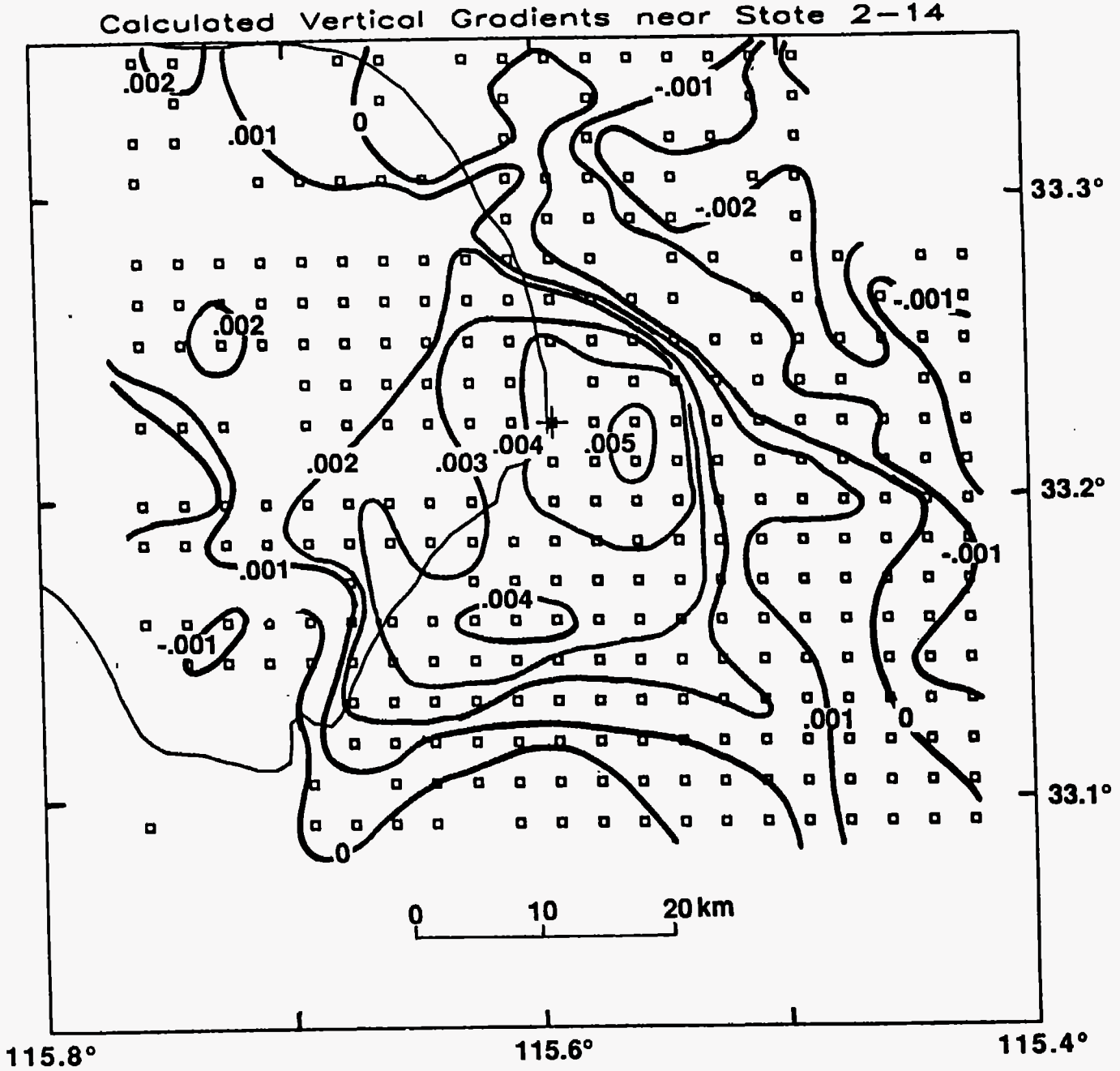
Calculated Vertical Gradients near State 2-14
.002
.001
0
-.001
-.002
-.001
.002
.002
.003
.004
.005
.001
.004
-.001
.001
0
0
0
10
20 km
33.3°
33.2°
33.1°
115.8°
115.6°
115.4°

Fig 1

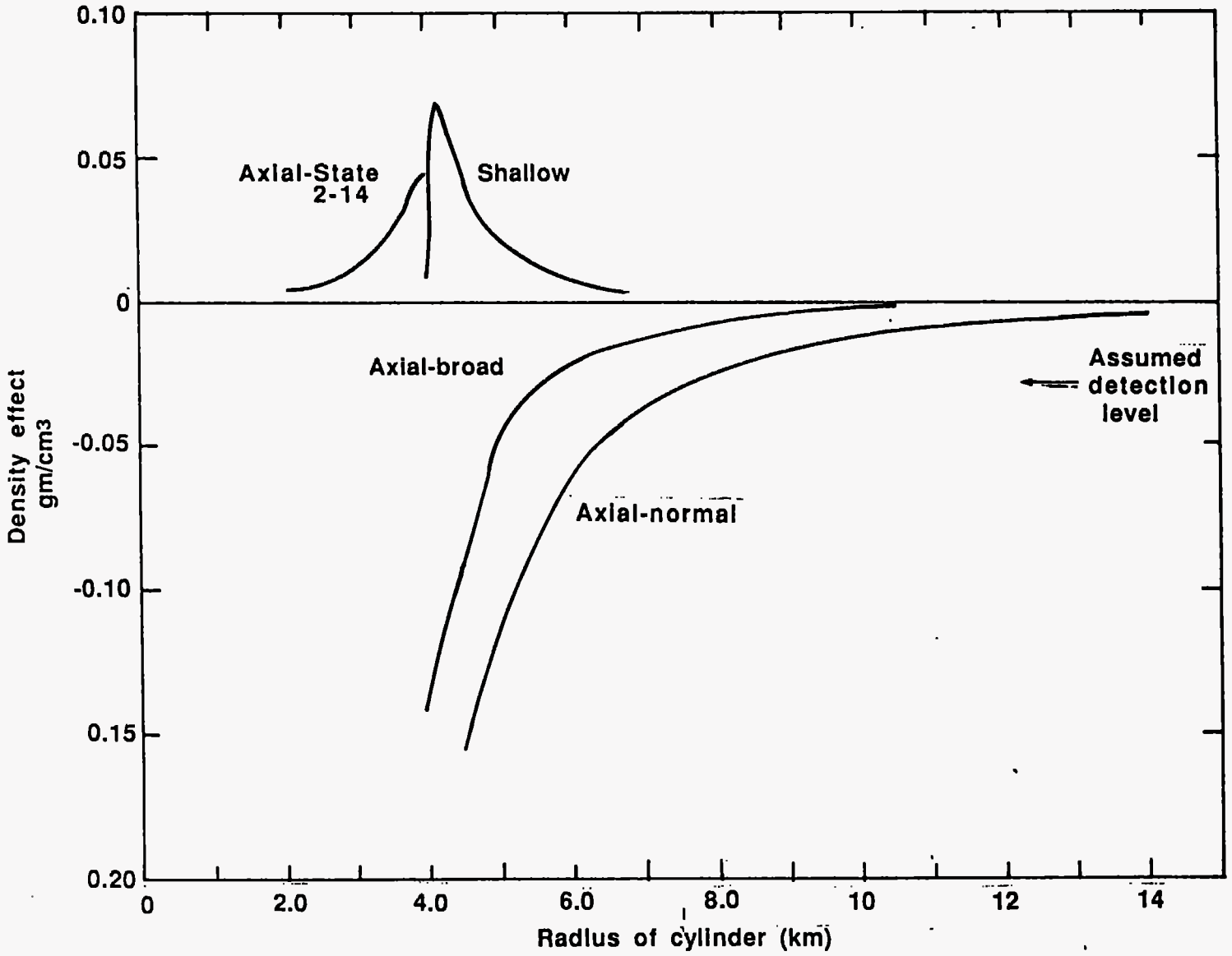
0.10
0.05
0
-0.05
-0.10
0.15
0.20
Density effect
gm/cm3
Axial-State
2-14
Shallow
Axial-broad
Axial-normal
Assumed
detection
level
0
2.0
4.0
6.0
8.0
10
12
14
Radius of cylinder (km)

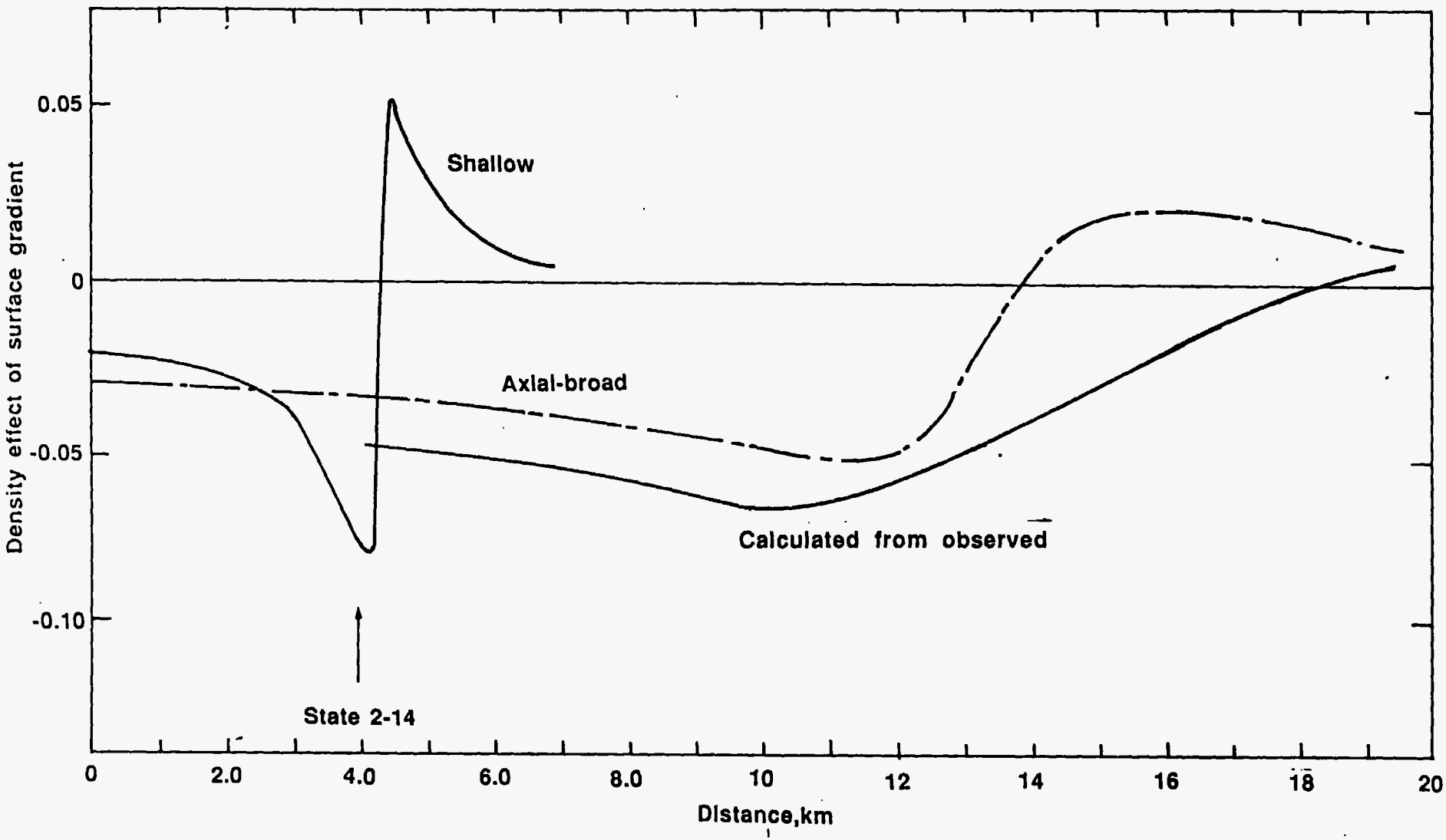
0.05
0
-0.05
-0.10
Density effect of surface gradient
Shallow
Axial-broad
Calculated from observed
State 2-14
0
2.0
4.0
6.0
8.0
10
12
14
16
18
20
Distance,km

Fig 8